Strong correlation between uniaxial magnetic anisotropic constant and in-plane tensile strain in Mn_4N epitaxial films

Cite as: AIP Advances **10**, 025117 (2020); https://doi.org/10.1063/1.5141818
Submitted: 08 December 2019 . Accepted: 28 January 2020 . Published Online: 11 February 2020

Taku Hirose, Taro Komori, Toshiki Gushi, Akihito Anzai, Kaoru Toko, and Takashi Suemasu

Strong correlation between uniaxial magnetic anisotropic constant and in-plane tensile strain in Mn_4N epitaxial films

Cite as: AIP Advances 10, 025117 (2020); doi: 10.1063/1.5141818
Submitted: 8 December 2019 • Accepted: 28 January 2020 •
Published Online: 11 February 2020

Taku Hirose,[1] Taro Komori,[1] Toshiki Gushi,[1,2] Akihito Anzai,[1] Kaoru Toko,[1] and Takashi Suemasu[1,a)]

AFFILIATIONS

[1]Institute of Applied Physics, Graduate School of Pure and Applied Sciences, University of Tsukuba, Tsukuba, Ibaraki 305-8573, Japan

[2]Université Grenoble Alpes, CNRS, CEA, Grenoble, SPINTEC, 38000 Grenoble, France

[a)]**Author to whom correspondence should be addressed:** suemasu@bk.tsukuba.ac.jp

ABSTRACT

Ferrimagnetic Mn_4N is a promising candidate for current-induced domain wall motion assisted by spin-transfer and spin–orbit torques. Mn_4N can be doped to have perpendicular magnetic anisotropy (PMA) and a small spontaneous magnetization. However, the origin of the PMA of Mn_4N has yet to be fully understood. Here, we investigated the relationship between the ratios of the perpendicular lattice constant c to the in-plane lattice constant a of Mn_4N epitaxial thin films (c/a) and the uniaxial magnetic anisotropic constant (K_u) in Mn_4N thin films grown on MgO(001), $SrTiO_3$(001), and $LaAlO_3$(001) substrates. The lattice mismatches between Mn_4N and these substrates are approximately −6%, −0.1%, and +2%, respectively. All the Mn_4N thin films had PMA and in-plane tensile distortion ($c/a < 1$) regardless of the Mn_4N thickness and substrate. Although the magnitude of c/a depended on several factors, such as the Mn_4N layer thickness and substrate, we found a strong correlation between c/a and K_u; K_u increased markedly when c/a deviated from 1. This result indicates that the origin of PMA is tensile distortion in Mn_4N films; hence, it might be possible to control the magnitude of K_u by tuning c/a through the Mn_4N layer thickness and the substrate.

I. INTRODUCTION

Nonvolatile memory devices with fast operation, low power consumption, and high-density information storage would be highly desirable. Racetrack memory is considered to be a promising candidate for realizing these requirements.[1] The physics of spin torque are based on the transfer of angular momentum to the magnetization. The flow of angular momentum is caused by a spin-polarized current in the case of spin-transfer torque (STT)[2,3] or arises from spin–orbit interactions, such as the spin Hall effect or the Edelstein–Rashba effect[4,5] in the case of spin–orbit torque. Magnetization switching is easily achieved for materials with a small spontaneous magnetization (M_S) because the drift velocity of domain walls (DWs) is inversely proportional to M_S.[6] These properties have renewed research interest in ferrimagnets.[7–10] In particular, current-induced domain wall motion (CIDWM) is faster in antiferromagnetic[11,12] and ferrimagnetic[13,14] materials than in ferromagnetic materials. Perpendicular magnetic anisotropy (PMA) is essential for CIDWM because materials with PMA generally have Bloch DWs, which contribute to faster DW motion with a smaller current.[15] Thus, we have focused our efforts on rare-earth free ferrimagnetic Mn_4N films. Mn_4N thin films have been grown on various substrates, such as glass,[16] Si(001),[17] and MgO,[18] by reactive sputtering. Mn_4N films have also been grown on MgO(001),[19] $SrTiO_3$[STO](001),[19] $(LaAlO_3)_{0.3}(Sr_2TaAlO_6)_{0.7}$(001),[20] 6H–SiC(0001),[21] and GaN(0001)[21] substrates by molecular beam epitaxy (MBE). Recent experiments have shown that when Mn_4N films exhibit PMA, the ratio of the perpendicular lattice constant c to the in-plane lattice constant a, c/a, is approximately 0.99, regardless of the lattice mismatch to various substrates.[19,22,23] The origin of PMA has long been investigated for ferrimagnets such as FePt, FePd, and Mn–Ga, wherein

in-plane tensile distortion was reported.[24–27] Therefore, Mn_4N thin films are considered to belong to the existing family of PMA materials with $c/a < 1$. The uniaxial magnetic anisotropy constant (K_u) of Mn_4N films has been reported to be approximately 10^5 J/m^3.[17,23,28] In addition, Mn_4N has a relatively small M_S of approximately 100 kA/m.[16,28–30] We achieved a record velocity of 900 m/s for a Mn_4N nanowire grown on $SrTiO_3$(001) without applying an external magnetic field.[31] Recently, considerable progress has been made in research of mixed crystals based on Mn_4N. We have reported magnetic compensation of $Mn_{4-x}Ni_xN$ between $x = 0.1$ and 0.25 at room temperature (RT).[32,33] A much faster DW velocity can thus be expected in such strips. Recent studies on how the nitrogen atoms and the layer thickness of Mn_4N contribute to PMA deepen the understanding of the fundamental properties of Mn_4N films.[34,35] However, there have been no systematic studies of the relationship between c/a and K_u in Mn_4N epitaxial films, although the origin of PMA is likely to be in-plane tensile distortion in Mn_4N films. Previously, we have grown Mn_4N thin films only on substrates that induce in-plane tensile distortion ($c/a < 1$), such as MgO and STO, from the viewpoint of lattice mismatch between Mn_4N and the substrates. However, no studies have been performed on Mn_4N thin films formed on substrates that might induce in-plane compressive distortion ($c/a > 1$) in Mn_4N films. Hence, in this paper, we systematically investigated the relationship between c/a and K_u to understand the origin of PMA. The lattice mismatches between Mn_4N and MgO(001), STO(001), and $LaAlO_3$[LAO](001) substrates are approximately −6%, −0.1%, and +2%, respectively, assuming that the Mn_4N film has a cubic structure and a lattice constant of 0.3865 nm,[30] which is the same lattice constant as bulk Mn_4N at RT. In this article, we found a strong correlation between c/a and K_u values in Mn_4N films, meaning that the K_u can be controlled by c/a.

II. EXPERIMENTAL

We grew Mn_4N thin films on MgO(001), STO(001), and LAO(001) substrates by MBE. The substrate temperature was set to be 450 °C and Mn was supplied from a Knudsen cell and N from a radio-frequency plasma. After growth, we observed the surface morphology by reflection high-energy electron diffraction (RHEED) and sputtered a 2–5 nm-thick SiO_2 as a capping layer to prevent oxidation. We used x-ray diffraction (XRD, Smart Lab, Rigaku, Inc., Japan) to assess the crystalline quality of the grown films. A Cu-$K\alpha$ radiation source was used for XRD and Ge(220) single crystals were used to monochromatize the x-ray beams. Lattice constants were identified from the angles of diffraction peaks in the out-of-plane and in-plane XRD profiles. In-plane lattice constants were calculated from the diffraction peaks of Mn_4N 100, 200, and 400 and perpendicular lattice constants were calculated from those of Mn_4N 001, 002, and 004. The lattice constant of the a-axis was the same as that of the b-axis because we confirmed that all samples had in-plane four-fold rotational symmetry from the ϕ-scan. The thickness of the grown films was measured by the x-ray reflectivity (XRR) method. Table I lists the sample preparation details, such as the substrate and grown layer thickness (t_{Mn4N}).

We used vibrating sample magnetometry (VSM) to measure magnetization vs magnetic field (M-H) loops at RT. The M_S was calculated from saturation regions of the M-H loops after demagnetizing field correction. The area of the samples was calculated with the use of ImageJ software, and the volume was determined to be the product of the area and the thickness from XRR. We used K_u to reflect the degree of PMA in this work. The values of K_u and the effective magnetic anisotropy constant (K_u^{eff}) were calculated from Eqs. (1)[36] and (2),[37]

TABLE I. Growth condition of Mn_4N thin films on MgO(001), STO(001), and LAO(001) substrates. Substrate and thickness of the Mn_4N (t_{Mn4N}) layer of the samples. Lattice constants c and a, and the ratio c/a are specified.

Sample	Substrate	t_{Mn4N} (nm)	c (nm)	a (nm)	c/a
Sample 1	MgO	11.6	0.3856	0.3884	0.9927
Sample 2	MgO	18.4	0.3862	0.3891	0.9927
Sample 3	MgO	42.4	0.3872	0.3890	0.9953
Sample 4	STO	7.4	0.3856	0.3908	0.9866
Sample 5	STO	17.1	0.3863	0.3907	0.9885
Sample 6	STO	39.4	0.3862	0.3911	0.9874
Sample 7	LAO	19.2	0.3866	0.3874	0.9979
Sample 8	LAO	39.4	0.3856	0.3871	0.9962

$$K_u = K_u^{eff} + \frac{\mu_0}{2} M_S^2, \tag{1}$$

$$K_u^{eff} = \left(\mu_0 \int_0^{M_S} H\, dM\right)_{hard} - \left(\mu_0 \int_0^{M_S} H\, dM\right)_{easy}, \tag{2}$$

where easy (hard) refers to the easy (hard) magnetization axis. The $\mu_0 {M_S}^2/2$ term in Eq. (1) is the demagnetization component. It was impossible to correctly calculate these constants from the measured M–H loops, because in our system, we could not apply the sufficient magnetic field to make the magnetization saturated in the in-plane direction. Thus, we used the fact that the loops acquired from the anomalous Hall effect (AHE) measurements correspond to the M–H loops measured by VSM. We calculated the subtractions of the loops from the AHE using Eqs. (1) and (2). Additionally, we calculated $M_{||}$ using Eq. (3),

$$M_{||} = M_S \sqrt{1 - \left(\frac{M_\perp}{M_S}\right)^2}, \tag{3}$$

where $M_{||}$ ($M_\perp$) is the in-plane (vertical) component of the magnetization. AHE measurements were performed with a physical property measurement system (Quantum Design). We applied magnetic fields of 3 T in the perpendicular direction and 9 T in the in-plane direction to measure the anomalous Hall signals. We determined the Hall resistivity (ρ_{xy}) from the transverse voltage (V_y) and the longitudinal current (I_x) with the use of Eq. (4),[38]

$$V_y = \left(R_H \frac{B_z}{t} + \frac{\rho_{AH}}{t} \frac{M_\perp}{M_S}\right) I_x = \frac{\rho_{xy}}{t} I_x, \tag{4}$$

where R_H, B_z, ρ_{AH}, and t are the ordinary Hall coefficient, the magnetic flux density perpendicular to the sample surface, the anomalous Hall resistivity, and the film thickness, respectively. We did not consider the planar Hall effect because the anisotropic magnetoresistance of the Mn_4N thin film was negligibly small at RT.[18] The slope in the high-H region, where M saturated, corresponds to the first

term in Eq. (4). Thus, we can subtract the contribution of this term from the measured value.

III. RESULTS AND DISCUSSION

Figure 1 shows out-of-plane XRD profiles and RHEED images of the samples on MgO, STO, and LAO substrates, respectively. In Fig. 1(a), Mn_4N 002 and 004 diffraction peaks appear in the samples on MgO substrates. Streaky patterns and superlattice diffraction lines, marked by white arrows, also appear in the RHEED images of Mn_4N films on MgO. The appearance of superlattice diffraction lines implies that a nitrogen atom is positioned at the body-center position in each lattice.[39] Mn_4N 002 and 004 diffraction peaks appear in the out-of-plane XRD profiles for Mn_4N films on STO as well as on MgO. Moreover, the streaky lines appearing in the RHEED images of Mn_4N films on STO are sharper than those on MgO. In Fig. 1(c), we observed Mn_4N 002 and 004 diffraction peaks in the out-of-plane XRD profiles of Mn_4N thin films on LAO. Although the RHEED image of sample 8 was not obtained because of mechanical issues, the RHEED image of sample 7 indicated a spotty pattern and rings, which suggested the formation of polycrystalline Mn_4N films.

Figures 2(a)–2(c) show the in-plane XRD profiles of Mn_4N thin films on MgO, STO, and LAO substrates, respectively. In Fig. 2(a),

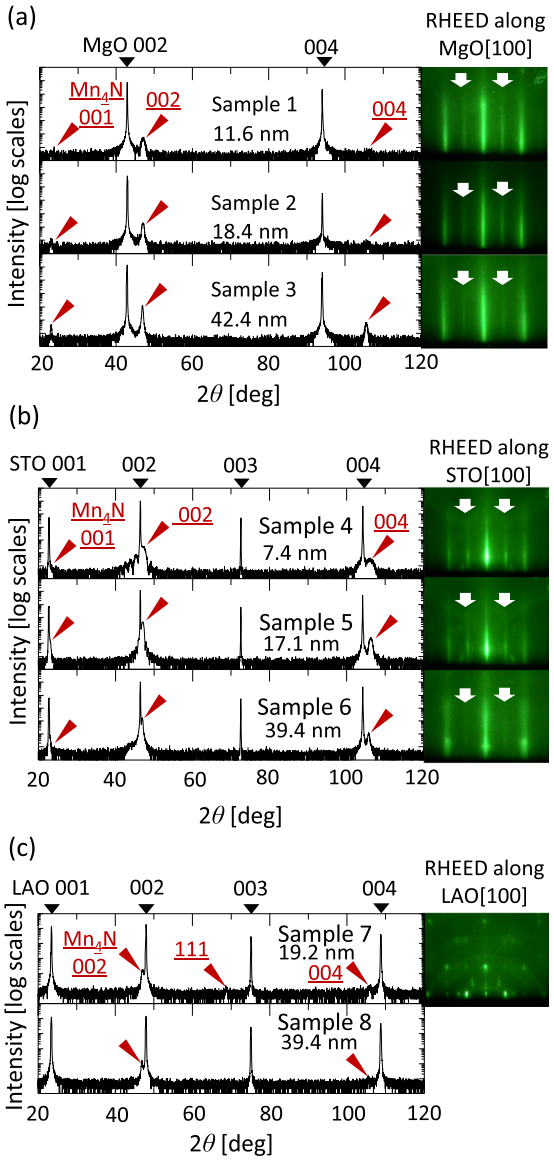

FIG. 1. Out-of-plane XRD profiles and RHEED images of Mn_4N thin films along the substrate [100] azimuth on (a) MgO(001), (b) STO(001), and (c) LAO(001) substrates. Black and red triangles show diffraction peaks of substrates and Mn_4N, respectively. In the RHEED images, white arrows indicate superlattice diffraction lines. Mn_4N layer thicknesses are shown.

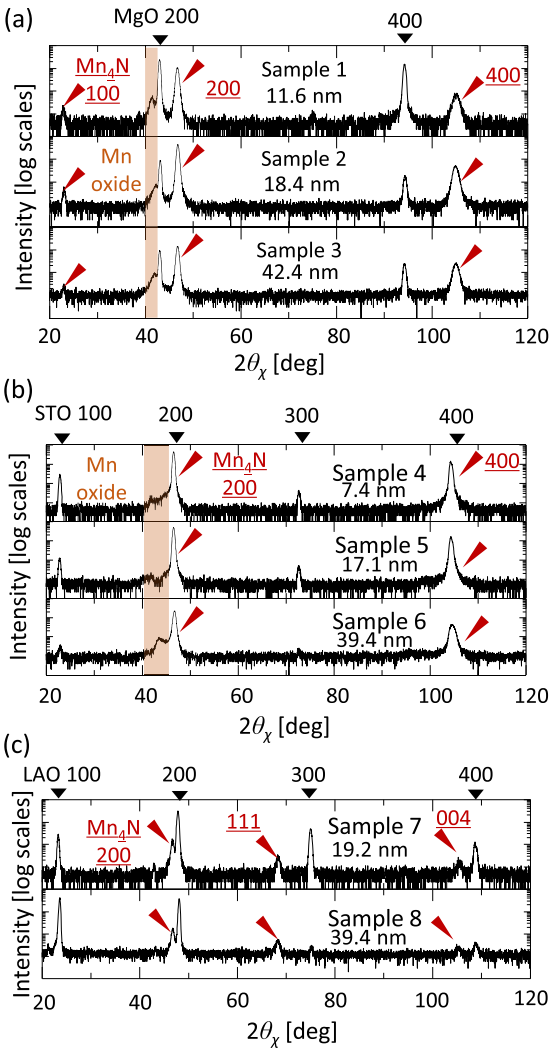

FIG. 2. In-plane XRD profiles of Mn_4N thin films on (a) MgO(001), (b) STO(001), and (c) LAO(001) substrates. Black and red triangles indicate diffraction peaks of substrates and Mn_4N, respectively. Mn_4N layer thicknesses are shown.

Mn_4N 100, 200, and 400 peaks of Mn_4N appeared in all the samples on MgO. Peaks of manganese oxide were also observed at $2\theta_\chi \sim 41°$ regardless of the substrate. These features might arise from the diffusion of oxygen atoms from SiO_2 cap layers. Regarding the Mn_4N films on STO, the lattices of Mn_4N and STO are well-matched. Hence, the 200 and 400 peaks of STO overlap those of Mn_4N in Fig. 2(b). For the Mn_4N films (t_{Mn_4N} = 39.4 nm) in sample 6, the 400 peak at $2\theta_\chi \sim 105°$ became broader. This is because the peak intensity of Mn_4N increased with t_{Mn_4N}, positioned at a little higher $2\theta_\chi$ than that of STO, making the peak broader. Actually, the measured peak profile was well reproduced by two pseudo-Voigt curves, and we determined the lattice constant a of Mn_4N films in this way. In Fig. 2(c), the 200 and 400 peaks of Mn_4N appeared in samples 7 and 8; however, the 111 peak of Mn_4N also appeared. Thus, we consider that it is difficult to grow Mn_4N epitaxially on LAO at 450 °C.

Figure 3 shows the relationship between the in-plane lattice constant a, the out-of-plane lattice constant c, and c/a against film thickness. Note that values of c/a are smaller than 1 for all the samples. We next focused our attention on Mn_4N films on MgO and STO substrates, which might induce in-plane tensile strain in Mn_4N, such that c/a increases with increasing t_{Mn_4N} and approaches 1. Note that c/a is closer to 1 for Mn_4N films on MgO than those on STO meaning that the lattice of Mn_4N films on MgO is more easily relaxed than those on STO. This phenomenon suggests that a Mn_4N thin film on MgO has more misfit dislocations in the vicinity of the interface because of the greater lattice mismatch,[40] whereas films on STO are highly epitaxial, according to cross-sectional transmission electron microscope (TEM) images.[23,31] In contrast, for the samples on LAO, a different trend was observed; c/a decreased with t_{Mn_4N}, likely because Mn_4N films on LAO are polycrystalline. Notably, c/a was less than 1 for all samples even on LAO substrates. We attribute this result to the fact that crystal structures with $c/a < 1$ are stable in the Mn_4N thin films based on theoretical calculations of the structural relaxation.[22]

Figure 4(a) shows ρ_{AH}–H loops measured under perpendicular magnetic fields for samples 2, 5, and 7, that is, Mn_4N films with t_{Mn_4N} = 18.4 nm, 17.1 nm, and 19.2 nm on MgO, STO, and LAO substrates, respectively. The loop of Mn_4N thin films on STO was the most well-squared (red), followed by those on MgO (blue). The squareness of the loops was poorest for the samples on LAO (black). These results show that the sharp magnetization reversal occurs in Mn_4N films on STO, whereas the slow magnetization reversal occurs in Mn_4N films on MgO and LAO. In other words, the magnetization reversal occurs in Mn_4N films on STO by a nucleation followed by an easy propagation. The inset of Fig. 4(a) shows the relationship between the ratio of the remanence magnetization to the spontaneous magnetization (M_r/M_S) vs Mn_4N film thickness.

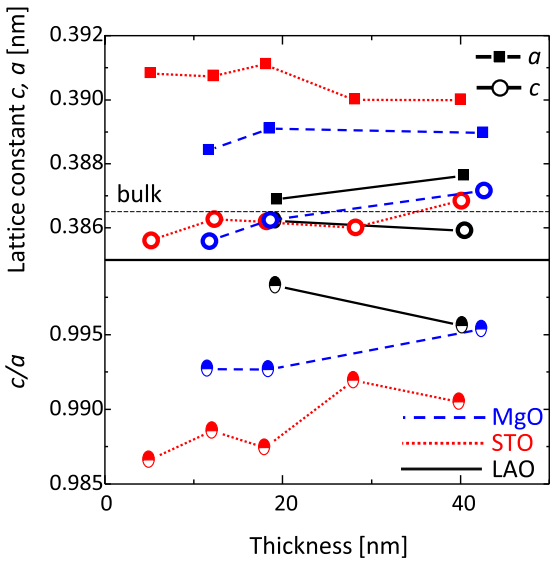

FIG. 3. Relationship between the in-plane lattice constant a, out-of-plane lattice constant c, and c/a against film thickness.

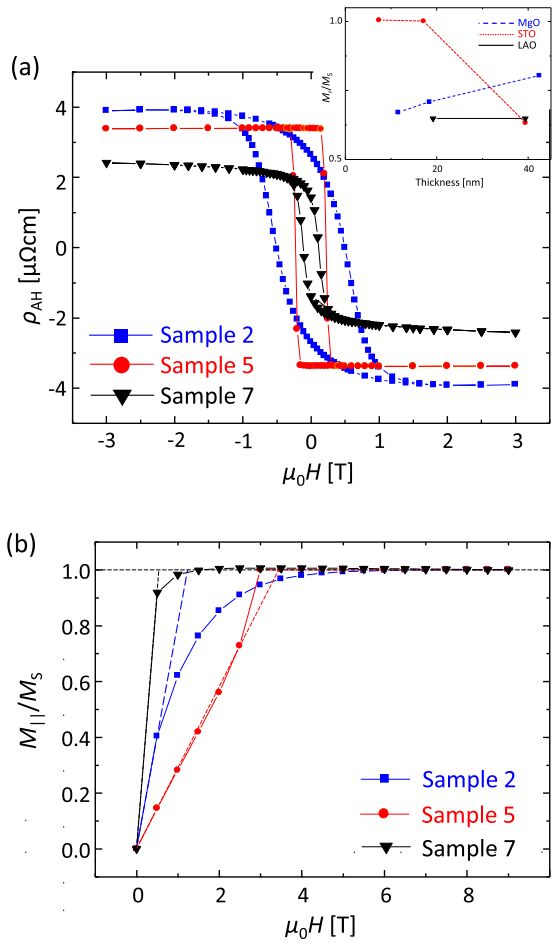

FIG. 4. (a) AHE loops measured at RT for Mn_4N films on MgO (blue squares, sample 2, t_{Mn4N} = 18.4 nm), STO (red circles, sample 5, t_{Mn4N} = 17.1 nm), and LAO (black inverted triangles, sample 7, t_{Mn4N} = 19.2 nm) substrates with H applied perpendicular to the plane. The inset shows the ratio of remanence magnetization to spontaneous magnetization (M_r/M_S) dependence on film thickness. (b) In-plane components of magnetization obtained from AHE measurements for samples in (a). Broken lines show the tangent when the field was 0 T.

Furthermore, the coercivity field of sample 7 was much smaller than those of samples 2 and 5. This trend is attributed to the small K_u and M_S values of the Mn_4N thin films on the LAO substrates. Figure 4(b) shows the normalized in-plane magnetization response when an in-plane magnetic field was applied. Figure 4(b) suggests that the magnetization saturated for a small field in the order sample 7 first, followed by sample 2, and then sample 5. Therefore, we can state that PMA appears in all the samples although the magnetic anisotropic constant is higher in Mn_4N thin films on substrates that induce in-plane tensile distortion. Table II summarizes M_S, K_u, the anisotropic field (H_K) calculated from Eq. (5), and that from the extrapolation of the gradient at $\mu_0 H = 0$ T (H_K'), as shown by the broken lines in Fig. 4(b),

$$H_K = \frac{2K_u}{M_S}. \quad (5)$$

From Table II, the values of H_K of both methods are almost the same for the samples on MgO and STO substrates. However, the values are different in the samples on LAO substrates. This difference derives from the deterioration of remanence magnetization of the samples on LAO.

Figure 5 shows the relationship between K_u and c/a. We confirmed that K_u becomes smaller when c/a approaches 1 in all the Mn_4N films, regardless of the substrates. We note here that the data points are on one broken line (gray), although the dependence of K_u on c/a differed markedly between samples. In particular, K_u changed markedly in Mn_4N films on STO. This is because the magnitude of c/a varied over a wide range from 0.985 to 0.995. In contrast, the change in c/a was limited to a smaller range for Mn_4N films on MgO and LAO. We posit that this difference originates from the difference in the lattice mismatch to Mn_4N at the interface. Misfit dislocations readily occurred in the vicinity of the interface because the lattice mismatch between Mn_4N and MgO is large ($\Delta a/a \approx -6\%$), even in thin films, leading to relaxation of the Mn_4N lattice.[23] Conversely, for Mn_4N films on STO, the lattice mismatch is sufficiently small ($\Delta a/a \sim -0.1\%$), and the absence of dislocations, perfect epitaxy, and sharp interface at Mn_4N/STO were confirmed by TEM.[31] Therefore, a large amount of tensile distortion ($c/a = 0.990$) remained, even in 40 nm-thick Mn_4N films, as shown in Fig. 3. Note that the complex magnetic structures such as local noncollinear magnetic order caused by dislocations around Mn_4N/substrate interfaces and nitrogen deficiencies, especially in the case of the Mn_4N film on MgO substrates, could influence the obtained K_u values. On the basis of these results, we conclude that the PMA in Mn_4N epitaxial films originated from tensile distortion ($c/a < 1$) and that K_u can be controlled by the magnitude of c/a.

TABLE II. Spontaneous magnetizations (M_S), uniaxial anisotropic constant (K_u), anisotropic field (H_K) calculated with the use of Eq. (5), and that obtained from the extrapolation of the gradient at $\mu_0 H = 0$ T (H_K').

Sample	M_S (kA/m)	K_u (MJ/m^3)	$\mu_0 H_K$ (T)	$\mu_0 H_K'$ (T)
Sample 1	80	0.052	1.3	1.4
Sample 2	63	0.060	1.9	1.6
Sample 3	78	0.041	1.1	1.2
Sample 4	78	0.215	5.5	5.2
Sample 5	73	0.126	3.5	3.6
Sample 6	73	0.049	1.3	1.2
Sample 7	53	0.045	1.7	0.6
Sample 8	59	0.051	1.7	0.6

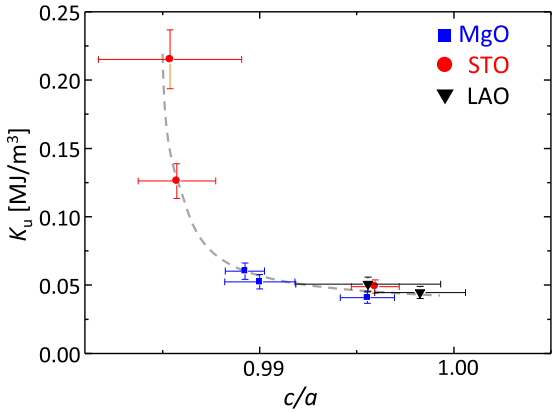

FIG. 5. Relationship between K_u and c/a. Blue square points, orange circle points, and black-triangular points show the data obtained from Mn_4N films on MgO(001), STO(001), and LAO(001), respectively. Broken gray line is a guide to the eyes.

IV. CONCLUSION

We grew 7–40 nm-thick Mn_4N thin films on MgO(001), STO(001), and LAO(001) substrates by MBE and investigated the relationship between the ratio of the perpendicular lattice constant to the in-plane lattice constant (c/a) in Mn_4N thin films and the uniaxial magnetic anisotropic constant (K_u). The K_u values were determined from anomalous Hall effect measurements at room temperature. All the Mn_4N films showed PMA and $c/a < 1$ even those on LAO(001) substrates, for which we initially expected compressive distortion ($c/a > 1$) to Mn_4N. Data points of K_u vs c/a are plotted on one line despite the dependence of K_u on c/a differing considerably between samples. The value of K_u increased markedly when c/a deviated from 1. Hence, we conclude that the origin of PMA in Mn_4N films is tensile distortion and that the value of K_u can be tuned by controlling c/a.

ACKNOWLEDGMENTS

The magnetic properties were measured with the help of Professor H. Yanagihara of the University of Tsukuba. Anomalous Hall effect measurements were performed with the use of a physical property measurement system with the help of Associate Professor T. Koyano of the Cryogenics Division of the University of Tsukuba. This work was financially supported by JSPS KAKENHI (Nos. 19K21954, 19KK0104, and 19K04499).

REFERENCES

[1] S. S. P. Parkin, M. Hayashi, and L. Thomas, Science **320**, 190 (2008).
[2] L. Berger, J. Appl. Phys. **49**, 2156 (1978).
[3] J. C. Slonczewski, J. Magn. Magn. Mater. **159**, L1 (1996).
[4] I. M. Miron, K. Garello, G. Gaudin, P. J. Zermatten, M. V. Costache, S. Auffret, S. Bandiera, B. Rodmacq, A. Schuhl, and P. Gambardella, Nature **476**, 189 (2011).

[5]L. Liu, C. F. Pai, Y. Li, H. W. Tseng, D. C. Ralph, and R. A. Buhrman, Science **336**, 555 (2012).
[6]A. Thiaville, Y. Nakatani, J. Miltat, and Y. Suzuki, Europhys. Lett. **69**, 990 (2005).
[7]M. Binder, A. Weber, O. Mosendz, G. Woltersdorf, M. Izquierdo, I. Neudecker, J. R. Dahn, T. D. Hatchard, J.-U. Thiele, C. H. Back, and M. R. Scheinfein, Phys. Rev. B **74**, 134404 (2006).
[8]J. Lu, S. W. Mao, X. P. Zhao, X. L. Wang, J. Liu, J. B. Xia, P. Xiong, and J. H. Zhao, Sci. Rep. **7**, 16990 (2017).
[9]J. Cui, M. Kramer, L. Zhou, F. Liu, A. Gabay, G. Hdipanayis, B. Balasubramanian, and D. Sellmyer, Act Mater **158**, 118 (2018).
[10]L. Caretta, M. Mann, F. Büttner, K. Ueda, B. Pfau, C. M. Günther, P. Hessing, A. Churikova, C. Klose, M. Schneider, D. Engel, C. Marcus, D. Bono, K. Bagschik, S. Eisebitt, and G. S. D. Beach, Nat. Nanotechnol. **13**, 1154 (2018).
[11]C. O. Avci, E. R. Baumgartner, L. Beran, A. Quindeau, P. Gambardella, C. A. Ross, and G. S. D. Beach, Appl. Phys. Lett. **111**, 072406 (2017).
[12]S.-H. Yang, K.-S. Ryu, and S. Parkin, Nat. Nanotechnol. **10**, 221 (2015).
[13]T. Komine, K. Takahashi, A. Ooba, and R. Sugita, J. Appl. Phys. **109**, 07D503 (2011).
[14]K.-J. Kim, S. K. Kim, Y. Hirata, S.-H. Oh, T. Tono, D.-H. Kim, T. Okuno, W. S. Ham, S. Kim, G. Go, Y. Tserkovnyak, A. Tsukamoto, T. Moriyama, K.-J. Lee, and T. Ono, Nat. Mater. **16**, 1187 (2017).
[15]S. Emori and G. S. D. Beach, Appl. Phys. Lett. **98**, 132508 (2011).
[16]K. M. Ching, W. D. Chang, and T. S. Chin, J. Alloys Compd. **222**, 184 (1995).
[17]D. Fruchart, D. Givord, P. Convert, P. l'Heritier, and J. P. Senateur, J. Phys. F: Metal Phys. **9**, 2431 (1979).
[18]K. Kabara and M. Tsunoda, J. Appl. Phys. **117**, 17B512 (2015).
[19]Y. Yasutomi, K. Ito, T. Sanai, K. Toko, and T. Suemasu, J. Appl. Phys. **115**, 17A935 (2014).
[20]T. Hirose, T. Komori, T. Gushi, K. Toko, and T. Suemasu, "Perpendicular magnetic anisotropy in ferrimagnetic Mn_4N films grown on $(LaAlO_3)_{0.3}(Sr_2TaAlO_6)_{0.7}(001)$ substrates by molecular beam epitaxy," J. Cryst. Growth (submitted).
[21]S. Dhar, O. Brandt, and K. H. Ploog, Appl. Phys. Lett. **86**, 112504 (2005).
[22]K. Ito, Y. Yasutomi, K. Kabara, T. Gushi, S. Higashikozono, K. Toko, M. Tsunoda, and T. Suemasu, AIP Adv. **6**, 056201 (2016).
[23]X. Shen, A. Chikamatsu, K. Shigematsu, Y. Hirose, T. Fukumura, and T. Hasegawa, Appl. Phys. Lett. **105**, 072410 (2014).
[24]A. Menshikov, T. Tarnoczi, and E. Kren, Phys. Status Solidi A **28**, K85 (1975).
[25]H. Niida, T. Hori, H. Onodera, Y. Yamaguchi, and Y. Nakagawa, J. Appl. Phys. **79**, 5946 (1996).
[26]M. Futamoto, M. Nakamura, M. Ohtake, N. Inaba, and T. Shimotsu, AIP Adv. **6**, 085302 (2016).
[27]B. S. Yang, L. N. Jiang, W. Z. Chen, P. Tang, J. Zhang, X. G. Zhang, Y. Yan, and X. F. Han, Appl. Phys. Lett. **112**, 142403 (2018).
[28]A. Anzai, F. Takata, T. Gushi, K. Toko, and T. Suemasu, J. Cryst. Growth **489**, 20 (2018).
[29]T. Komori, A. Anzai, T. Gushi, K. Toko, and T. Suemasu, J. Cryst. Growth **507**, 163 (2019).
[30]W. J. Takei, R. R. Heikes, and G. Shirane, Phys. Rev. **125**, 1893 (1962).
[31]T. Gushi, M. J. Klug, J. Pena Garcia, G. Sambit, J. P. Attane, H. Okuno, O. Fruchart, J. Vogel, T. Suemasu, S. Pizzini, and L. Vila, NANO Lett. **19**, 8716 (2019).
[32]T. Komori, T. Gushi, A. Anzai, L. Vila, J. P. Attene, S. Pizzini, J. Vogel, S. Isogami, K. Toko, and T. Suemasu, J. Appl. Phys. **125**, 213902 (2019).
[33]T. Komori, T. Hirose, T. Gushi, K. Toko, T. Hanashima, L. Vila, J.-P. Attanè, K. Amemiya, and T. Suemasu, J. Appl. Phys. **127**, 043903 (2020).
[34]A. Foley, J. Corbett, A. Khan, A. L. Richard, D. C. Ingram, A. R. Smith, L. Zhao, J. C. Gallagher, and F. Yang, J. Mag. Mag. Mater. **439**, 236 (2017).
[35]S. Isogami, K. Mauda, and Y. Miura, Phys. Rev. Mater. **4**, 014406 (2020).
[36]D. Ravelosona, A. Cebollada, F. Briones, C. Diaz-Paniagua, M. A. Hidalgo, and F. Batallan, Physica B **59**, 4322 (1999).
[37]K. Yamada, H. Kakizaki, K. Shimamura, M. Kawaguchi, S. Fukami, N. Ishiwata, D. Chiba, and T. Ono, Appl. Phys. Express **6**, 073004 (2013).
[38]F. Wu, S. Mizukami, D. Watanabe, H. Nagamura, M. Oogane, Y. Ando, and T. Miyazaki, Appl. Phys. Lett. **94**, 122503 (2009).
[39]K. Ito, S. Higashikozono, F. Takata, T. Gushi, K. Toko, and T. Suemasu, J. Cryst. Growth **455**, 66 (2016).
[40]T. Gushi, L. Vila, O. Fruchart, A. Marty, S. Pizzini, J. Vogel, F. Takata, A. Anzai, K. Toko, and T. Suemasu, Jpn. J. Appl. Phys. **57**, 120310 (2018).